Atomistic investigation on the impact of substitutional Al and Si atoms on the carbon kinetics in ferrite

Liangzhao Huang[a,*], Paul Eyméoud[b], Philippe Maugis[a]

[a] *Aix Marseille Université, CNRS, IM2NP, Marseille, France*
[b] *Université de Toulon, Aix Marseille Université, CNRS, IM2NP, Toulon, France*

Abstract

The pairwise interactions of substitutional solute atom X = Al, Si with interstitial carbon at stable (octahedral) and saddle-point (tetrahedral) positions in body-centered-cubic iron (α-Fe) are computed using density-functional theory. These pairwise interactions are used in atomistic kinetic Monte Carlo approach to simulate carbon internal friction and tracer diffusion measurements in Fe-Si, Fe-Al, and Fe-Al-Si ferritic alloys without any adjusting parameters. The good agreement between the simulated and experimental Snoek relaxation profiles validates the pair interaction model for kinetic simulations. The predicted effect of Al on slowing down carbon diffusion is consistent with previous studies. We highlight a super-cell size effect on the Si-carbon interactions obtained from first principles. Using a carefully tested database, it is shown that the introduction of Si into ferrite only decreases the carbon diffusivity below a critical temperature.

Keywords: Internal friction, tracer diffusion, first principles, Monte Carlo, Fe-Al-C, Fe-Si-C, Fe-Al-Si-C

1. Introduction

Fe-Si, Fe-Al and Fe-Al-Si are ferritic systems that have been widely studied because of their practical relevance. They are functional materials with favorable mechanical and magnetic properties. Carbon segregation and carbide formation play an essential role in the ageing of these ferritic systems [1, 2, 3, 4]. Therefore, the study of carbon diffusion is of particular importance. It is known that carbon kinetics is much affected by substitutional Si and Al atoms due to solute-carbon interactions [5, 6, 7, 8]. Multiple experimental studies attempted to investigate this solute effect by measuring the internal friction profiles in ferritic alloys [9, 10, 11, 12, 13, 14, 15, 16, 17]. This profile corresponds to the macroscopic signal of the carbon atomic jumps, which is sensitive to the change in activation enthalpies due to solute-carbon interactions [18, 15]. Therefore, internal friction profile characterizes well the behaviors of short-range carbon diffusion. However, in these alloys, the long-range diffusion of carbon with kinetic correlations has been much less studied experimentally.

High-performance *ab-initio* calculations make it possible to compute accurately the solute-carbon interactions [7, 8, 19, 20]. In the dilute limit, the exact calculation of carbon diffusivity is possible using available analytical approaches such as kinetic cluster expansions [21, 22]. In alloys with concentrated substitutional solute atoms, the general approach to study the short-range and long-range carbon kinetics is the atomistic kinetic Monte Carlo (AKMC) simulations [23, 7, 24, 19, 25]. In general, only pairwise solute-carbon interactions are considered in the simulation because *ab-initio* calculations for more complex clusters (e.g., triplet, quadruplet) requires very high computational cost.

Our objective is to perform quantitative studies on the short-range and long-range carbon diffusion in Fe-Si, Fe-Al and Fe-Al-Si ferritic systems following a multi-scale scheme, which is reflected in the outline of this paper. First, we will perform *ab-initio* calculations of pair interactions between substitutional atom X = Al, Si and carbon atoms at octahedral and tetrahedral (saddle-point) positions. Second, we will perform AKMC simulations of internal friction measurements in investigated alloys using a pair interaction model. The validation of this model will be justified by a comparison between the simulated and experimental Snoek profiles. Finally, using the same numerical approach, we will compute the tracer diffusion coefficients of carbon atoms in the investigated alloys.

2. Diffusion model

The three sets of non-equivalent octahedral (resp. tetrahedral) sites are characterized by the force dipole tensor $\boldsymbol{P}^{\mathrm{O}}_{i=1,2,3}$ (resp. $\boldsymbol{P}^{\mathrm{T}}_{j=1,2,3}$). Assuming that the carbon atoms are randomly distributed in space, the resulting strain field ($\boldsymbol{\epsilon}$) is given by a mean-field approach [26, 27] and is written

*Corresponding author
Email addresses: huang.liangzhao@outlook.com (Liangzhao Huang), paul.eymeoud@univ-tln.fr (Paul Eyméoud), philippe.maugis@im2np.fr (Philippe Maugis)

as:

$$\boldsymbol{\epsilon} = \boldsymbol{S}(\boldsymbol{\sigma} + \boldsymbol{p}), \tag{1}$$

where $\boldsymbol{S}$ is the elastic compliance tensor, $\boldsymbol{\sigma}$ is the stress tensor, and $\boldsymbol{p}$ is the average dipole tensor which is given by

$$\boldsymbol{p} = \frac{1}{V_0} \sum_{i=1}^{3} c_i \boldsymbol{P}_i^{\mathrm{O}}, \tag{2}$$

with V_0 the atomic volume of the lattice and c_i is the site fraction defined as the ratio between the number of carbon atoms sitting on the i-octahedral site and the number of bcc lattice sites. The migration enthalpy of a carbon atom from octahedral site i through the tetrahedral site j is expressed as function of the strain tensor and the elastic dipole tensors [28, 29, 30, 27]:

$$H_{i/j}^{\mathrm{m}} = H_0^{\mathrm{m}} - (\boldsymbol{P}_j^{\mathrm{T}} - \boldsymbol{P}_i^{\mathrm{O}}) : \boldsymbol{\epsilon}, \tag{3}$$

where H_0^{m} is the migration enthalpy of the stress-free bcc Fe crystal. This equation implies that the carbon diffusion enthalpy depends on both the applied stress $\boldsymbol{\sigma}$ and the carbon distribution.

In systems with substitutional solutes, the carbon migration enthalpy depends also on the local chemical environment. A pairwise interaction model is applied to describe the variation of the carbon migration barriers with the local environments. The X-C (X = Al, Si) pairwise interactions are given by the *ab initio* calculations. These interactions are included in the carbon jump frequency:

$$\omega_{i/j} = \nu_0 \exp\left[-\frac{H_{i/j}^{\mathrm{m}} + \sum_X (E_{X\text{-C}}^{\mathrm{T}} - E_{X\text{-C}}^{\mathrm{O}})}{k_{\mathrm{B}} T} \right], \tag{4}$$

where k_{B} is the Boltzmann constant, T is temperature, ν_0 is the attempt frequency that is assumed to be strain- and composition-independent, and

$$E_{X\text{-C}}^{\mathrm{T}} = \sum_k z_k V_{X\text{-C(T)}}^k, \; E_{X\text{-C}}^{\mathrm{O}} = \sum_k z_k V_{X\text{-C(O)}}^k, \tag{5}$$

where z_k is the number of atom X = Al, Si at the k-th nearest-neighbour shell of the considered carbon atom, and $V_{X\text{-C(T)}}^k$ [resp. $V_{X\text{-C(O)}}^k$] is the pairwise interaction between an atom X on a substitutional site and a carbon atom on a tetrahedral (resp. octahedral) site at the k-th nearest-neighbor distance.

3. Density functional theory calculations

We followed a similar numerical scheme as our previous work [20] to perform the density function theory (DFT) calculations of the X-C (X = Al, Si) pairwise interactions. First-principles calculations have been performed with VASP code [31, 32], with generalized gradient approximation [33] with projector augmented wave method [34] and Perdew-Burke-Ernzerhof exchange-correlation functionals [35, 36], spin polarized approximation, 550 eV energy cut-off, $4 \times 4 \times 4$ bcc supercell containing 127 Fe atoms, 1 X atom and 1 C atom (associated $6 \times 6 \times 6$ Monkhorst-Pack scheme [37] for k-points meshes construction), 10^{-8} eV energy convergence criterion for electronic self-consistency. To reproduce carbon migration paths, Climbing Image Nudged Elastic Band (CI-NEB) methodology has been used for fixed lattice volume and shape (only internal relaxations were allowed), with 9 intermediary images, and 0.05 eV/Å ionic relaxation criterion. We considered seven (resp. five) neighboring shells of octahedral (resp. tetrahedral) sites [cf. Fig. 1 (left)].

In Fig. 1 (middle and right), we compare the X-C pair interactions given by this work with those from different studies in the literature [7, 8, 38, 39]. Overall, the interactions of X = Al, Si with carbon atoms in octahedral sites obtained from this work are in relatively good agreement with other studies. As for the interactions of X with carbon atoms in tetrahedral sites, our results are in general smaller than those from Liu et al. We will discuss in Section 6.1 this difference and the resulting deviation in the predicted carbon diffusion properties.

Elastic parameters of α-Fe used in the following kinetic simulations are taken from our previous work [20], which are given in Tab. 1. The attempt frequency and the stress-free carbon migration enthalpy are obtained by fitting the data in Ref. [40]: $\nu_0 = 149$ THz and $H_0^{\mathrm{m}} = 0.872$ eV.

Table 1: Elastic parameters of α-Fe that are used in the kinetic simulations. These results were computed from first principles in Ref. [20].

Lattice parameter [Å]	2.831
S_{11} [GPa^{-1}]	0.00555
S_{12} [GPa^{-1}]	−0.00191
S_{44} [GPa^{-1}]	0.00100
P^{O}, transverse [eV]	9.1
P^{O}, longitudinal [eV]	18.2
P^{T}, transverse [eV]	14.3
P^{T}, longitudinal [eV]	5.0

4. Monte Carlo simulation

The internal friction and tracer diffusion are calculated by atomistic kinetic Monte Carlo (AKMC) simulations based on the residence-time algorithm. These simulations are performed on the body-centered cubic (bcc) lattice with the octahedral sites. Details of the method can be found in Refs. [27] and [25].

4.1. Internal friction

For the internal friction simulation, we consider a system submitted to a sinusoidal $(1\bar{1}0)[110]$ shear stress at selected frequency f such that $\sigma_{22} = -\sigma_{11} = \sigma_0 \sin(2\pi f t)$. The crystal response is a sinusoidal shear strain $\epsilon(t)$. The time

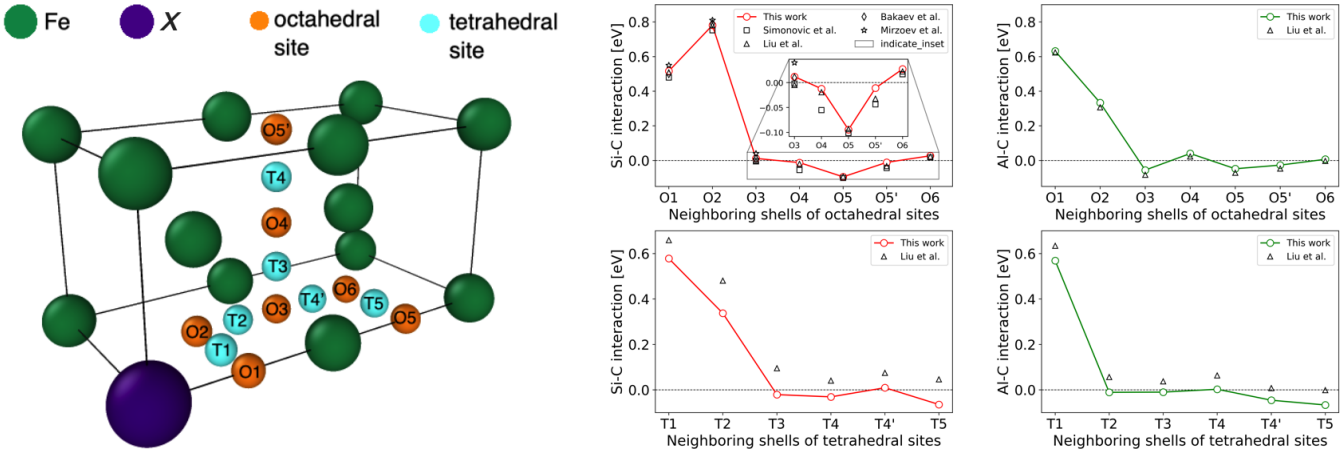

Figure 1: Left: Neighboring shells of octahedral and tetrahedral interstitial sites surrounding a substitutional solute atom X = Al, Si. Middle: Si-C pairwise interaction for C in octahedral (top) and tetrahedral (bottom) sites. Right: Al-C pairwise interaction for C in octahedral (top) and tetrahedral (bottom) sites. Positive pairwise interactions correspond to repulsive interactions.

lag between stress and strain corresponds to the energy loss of the system, i.e., the internal friction (denoted by Q^{-1}). The latter is computed as the fraction energy loss per cycle:

$$Q^{-1} = \frac{1}{2\pi}\frac{\Delta W}{W_{\max}}, \tag{6}$$

where $\Delta W = \int \boldsymbol{\sigma} : d\boldsymbol{\epsilon}$ is the energy loss per cycle and $W_{\max}$ is the maximum elastically stored energy per unit volume during a cycle. Note that if carbon atoms are diffusing in low-carbon Fe, Q^{-1} follows a Debye curve [18]:

$$Q^{-1} = \Delta\frac{\omega\tau}{1+(\omega\tau)^2}, \tag{7}$$

where $\omega = 2\pi f$, τ is the relaxation time, and Δ is the relaxation strength. It is shown in Ref. [41] that both τ and Δ depend on the material parameters, carbon content and temperature. At low carbon content, the relaxation time τ has a simplified expression [42, 19, 41]:

$$\tau = (6\nu_0)^{-1}\exp\left(\frac{H_0^{\mathrm{m}}}{k_{\mathrm{B}}T}\right). \tag{8}$$

Q^{-1} reaches its maximum when $\tau = 1/\omega$. According to Eq. (8), for a given relaxation frequency (f or ω), the temperature corresponding to the maximum Q^{-1} writes

$$T_{\max} = \frac{H_0^{\mathrm{m}}}{k_{\mathrm{B}}\ln(6\nu_0/\omega)}. \tag{9}$$

We introduce 1000 carbon atoms in the lattice. The size of the simulation box is adjusted by the atomic fraction of carbon atoms. The number of the substitutional solute atoms in the bcc lattice is set to a value so that the solute concentration equals the chosen one. The number of simulation steps is adjusted such that the number of stress cycles is larger than 50 in order to reach a good statistics. The applied stress amplitude is set to 300 MPa. The latter is a relatively high value compared with the experimental usage, but technically necessary to overcome the high fluctuations present in the finite-size simulation box [41]. The site fractions of the carbon atoms ($c_{i=1,2,3}$) are measured after each atomic jump. The resulting strain evolution $\epsilon(t)$ is given by the mean-field elastic model [27].

4.2. Tracer diffusion

For the tracer diffusion measurement, about 9 carbon atoms are inserted in the simulation box of 2×36^3 bcc sites (corresponding to a carbon concentration of 0.01 at.%). 1000 measurements of the mean squared displacement (MSD) of the carbon atoms after 9×10^6 atomic jumps (i.e., a total of 9×10^9 carbon jumps for each simulation) are performed to compute the tracer diffusion coefficients. The standard error of the obtained carbon diffusivities is within $\pm5\%$ with these settings. The tracer diffusivity D_{C} is related to the MSD $\langle R^2\rangle$ during a period of time τ via the Einstein-Smoluchowski equation: $\langle R^2\rangle = 6D_{\mathrm{C}}\tau$. The MSD is given by

$$\langle R^2\rangle = \left\langle\left(\sum_{n=1}^{N}R_n\right)^2\right\rangle = f_{\mathrm{C}}\left\langle\left(\sum_{n=1}^{N}R_n^2\right)\right\rangle, \tag{10}$$

where N is the total number of jumps in the period of time τ and R_n is the displacement of a carbon atom due to the n-th jumps. $\left\langle\left(\sum_{n=1}^{N}R_n^2\right)\right\rangle$ is the uncorrelated MSD corresponding to the random diffusion path, and f_{C} is the correlation factor characterizing the deviation between the tracer diffusion and a random walk. Note that the displacements of about 9 C atoms are simultaneously measured during the simulation. Therefore, the final MSD results from the average of all carbon atoms.

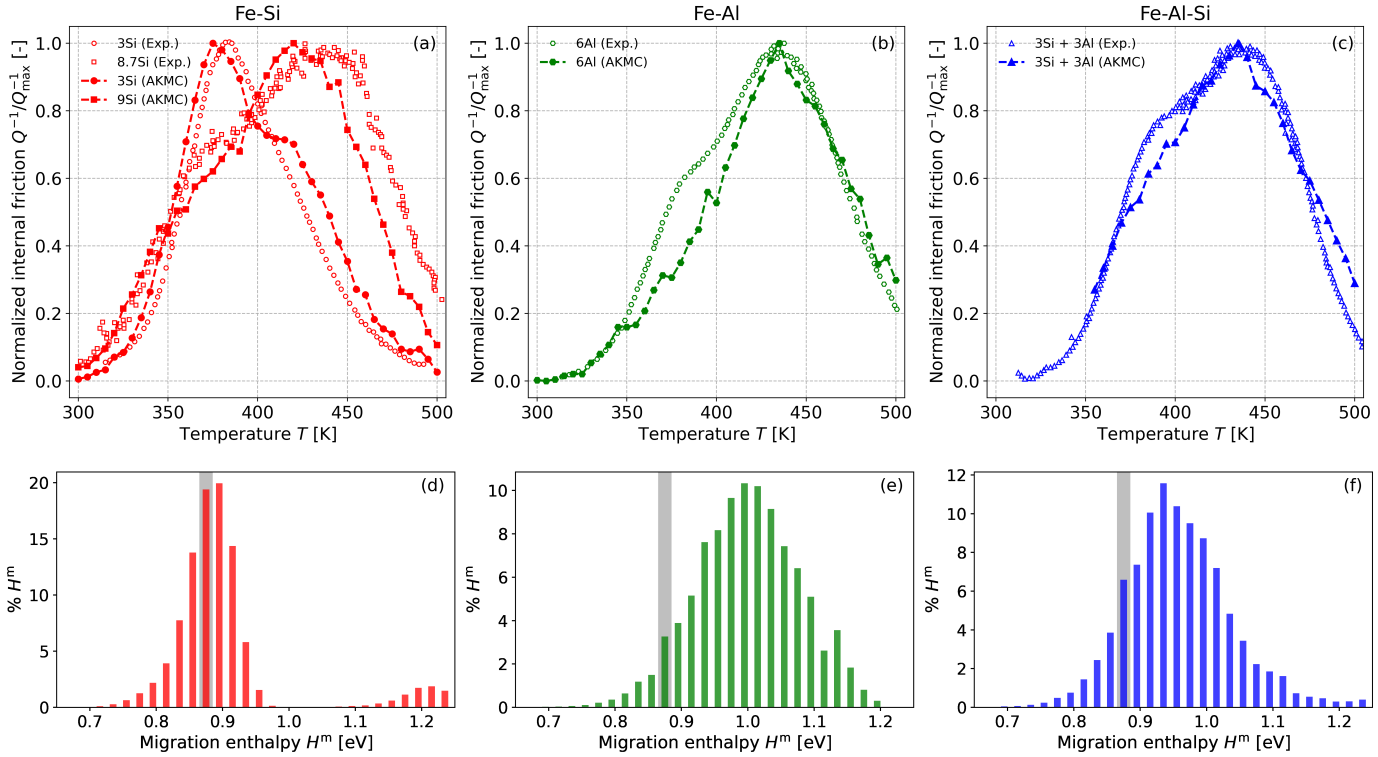

Figure 2: (a)–(c): Experimental and simulated carbon Snoek relaxation profiles in bcc Fe-Si, Fe-Al and Fe-Al-Si alloys. The alloy compositions are expressed in at.%. The experimental profiles are reproduced from the results of Sinning et al. [17], in which all the samples were water-quenched from 1000 K. The experimental excitation frequency of Fe-3Si and Fe-8.7Si systems is 320–410 Hz, and the one of Fe-6Al and Fe-3Al-3Si is about 600 Hz. The excitation frequency of AKMC simulation is set to 400 Hz for Fe-3Si and Fe-9Si, and 600 Hz for Fe-6Al and Fe-3Al-3Si. (d)–(f): Distribution of carbon migration enthalpy H^m in Fe-6Si, Fe-6Al and Fe-3Al-3Si alloys measured by AKMC simulation at 400 K. The shaded area indicates the carbon migration enthalpy in substitutional solute-free bcc Fe.

5. Results of carbon kinetics

5.1. Internal friction: validation of the pairwise interaction model

In Fig. 2 (a)–(c), we present the simulated temperature-dependent internal friction (TDIF) profiles in Fe-Si, Fe-Al and Fe-Al-Si alloys obtained by AKMC simulation. In order to validate the simulation approach of the Snoek relaxation process, we present also the experimental profiles obtained by Sinning et al. [17] and Golovin et al. [43]. The TDIF amplitude is mainly related to the carbon concentration and the elastic properties of the material. Here, we focus mainly on the TDIF peak temperatures, which are directly determined by the carbon migration enthalpy in the investigated alloys. The TDIF profiles are normalized by their maximum amplitude to avoid the influence of carbon concentration and elastic parameters. It is shown in Ref. [19] that the internal friction profiles are closely related to the distribution of carbon migration enthalpy in the alloy. Therefore, such distribution is measured by AKMC simulation and plotted in Fig. 2 (d)–(e) for a better understanding of the TDIF profile.

In Fig. 2 (a), we plot the simulated profiles in Fe-3Si and Fe-9Si, as well as the experimental ones in Fe-3Si and Fe-8.7Si. These profiles consist of two potential relaxation peaks: one at about 380 K, the other at about 415 K. The former peak temperature is almost the same as the one reported in α-Fe (the so-called Fe-C-Fe peak) at an excitation frequency of about 400 Hz [14] and thus, it corresponds to the carbon jumps far from solute Si atoms. Note that by applying Eq. (9), we obtain consistent result: this peak results mainly from the jump with migration enthalpy of 0.87 eV—the *ab initio* value of the carbon migration enthalpy in α-Fe and the most frequent value in the migration enthalpy distribution. The second peak results from short-range interactions between C and Si atoms—the so-called Fe-C-Si peak. Applying Eq. (9), we can roughly estimate the migration enthalpy related to this temperature peak, which is about 0.95 eV. However, this value does not correspond to one of the most frequent enthalpies in the distribution [cf. Fig. 2 (d)].

In the Fe-6Al alloy, the experimental profile consists of a peak at about 435 K and a shoulder at about 390 K [cf. Fig. 2 (b)]. The latter corresponds to the Snoek peak of carbon jumps in α-Fe (i.e. the Fe-C-Fe peak) at 600 Hz. According to the relation Eq. (9), the peak temperature of 435 K is consistent with the most frequent migration enthalpy (about 0.99 eV) of the distribution shown in Fig. 2 (e). Therefore, this peak results from carbon jumps near Al atoms (Fe-C-Al peak). In the simulated profile, the

Fe-C-Fe peak is not as visible as it is in the experimental profile, though the Fe-C-Al peak position is well reproduced.

As for the Fe-3Al-3Si system, the experimental profile is similar to the one of Fe-6Al alloy: it is composed of a peak at about 435 K and a shoulder at about 390 K. Once again, the latter corresponds to the Fe-C-Fe peak. The appearance of 435 K-peak should be due to the Al-C pair interactions because it appeared also in the profile of Fe-6Al alloy. Moreover, the profile of Fe-3Al-3Si alloy is wider than the one of Fe-6Al alloy because it comprises also a peak due to the Si-C pair interaction at about 405 K corresponding to the most frequent migration enthalpy in the distribution [cf. Fig. 2 (f)]. Accounting for only the pairwise interactions, AKMC simulations predict that the major peak is at about 435 K. This value corresponds well to the highest peak of the experimental profile.

Overall, the agreements between experimental and simulated profiles respective in Fe-Si, Fe-Al and Fe-Al-Si systems are satisfactory. This validates the use of the pairwise interaction model [i.e. Eq. (4)] to describe the dependence of carbon kinetics on the local alloy composition. Moreover, this confirms the Snoek nature of the experimental profiles, and therefore the C-Snoek peaks in Fe-Si alloys are not masked by the so-called 'P1' peak related to dislocation motions shown in Ref. [44].

5.2. Long-range carbon diffusion

In Fig. 3, we present the long-range diffusion properties of carbon in Fe-Si, Fe-Al and Fe-Al-Si alloys. We also compare these properties to those in α-Fe to highlight the substitutional solute effect on carbon diffusion.

In Fe-Si alloys, the tracer diffusion coefficients of carbon are close to those in α-Fe. The introduction of Si in Fe slightly increases the carbon diffusivity at 500–1000 K, while it reduces the diffusivity below 500 K. This decrease of carbon diffusivity results from the kinetic correlation at low temperature (i.e. the reduce of correlation factor) mainly due to a trapping mechanism at O5-configuration in which the Si-C interaction is attractive.

In Fe-Al alloys, the carbon diffusivity is much lower than that in α-Fe. The introduction of 3 at.% Al in Fe decreases the carbon diffusivity by about 20% at 1000 K, and by about an order of magnitude at room temperature; the introduction of 6 at.% Al in Fe reduces the carbon diffusivity by about 40% at 1000 K, and by more than an order of magnitude below room temperature. Compared with Si, Al has a more significant effect on the reduction of carbon diffusion because it has more attractive pair configurations (O3, O5, and O5'), which lead to stronger trapping effects and kinetic correlations.

In Fe-3Al-3Si, carbon diffusion is also slower than that in α-Fe mainly because of the introduction of 3 at.% Al, as the effect of 3 at.% Si on slowing down carbon diffusion is much smaller. The carbon diffusivity is reduced to 85% of the substitutional solute-free value $[D(C_X = 0)]$ at 1000 K and to 10% of $D(C_X = 0)$ at room temperature.

6. Discussions

6.1. Ab-initio energy database and KRA model

Simonovic et al. [7] have performed AKMC simulations to compute the carbon diffusivity in Fe-Si alloys. They showed that the introduction of 2 at% Si in Fe reduced the carbon diffusivity by about 20% at 500 K and by about 8% at 1000 K. Liu et al. [8] have performed similar studies in Fe-Si and Fe-Al alloys. They obtained that the introduction of 2 at% Si reduced the carbon diffusivity by about 80% at 500 K and by about 50% at 1000 K. In addition, they showed that Si is more efficient in slowing down carbon diffusion than Al. Their results are qualitatively and quantitatively different from what we predict. This difference originates from the following two aspects.

- The interactions of Si with carbon at octahedral sites obtained from Simonovic et al. and Liu et al. are different from our results. For example, compared with our results, they had more attractive O3, O4, and O5' configurations. Thus, the trapping mechanism due to Si is more significant with their energy database. However, our *ab initio* calculations are performed with a larger simulation box, in which the effects of periodic images on the pair interactions are much smaller. Focusing only on the energy of O3 configuration, we can see notable variations depending on the size of the supercell used for the DFT calculation. A slightly negative O3-interaction was obtained by Simonovic et al. (−0.002 eV) [7] and Liu et al. (−0.005 eV) [8] with a supercell of 54 atoms, while a slightly positive O3-interaction was obtained by Bakaev et al. (+0.01 eV) [38] and Mirzoev et al. (+0.04 eV) [39] with a supercell of 128 atoms as our work (+0.012 eV). Note that a similar size effect on the sign of carbon-carbon pair interactions computed by DFT has been revealed in [45].

- The interactions of Si with carbon at tetrahedral sites in Simonovic's work were obtained from an approximated approach—Kinetically-Resolved Activation (KRA) model [46]. However, the corresponding interactions are obtained from first principles in our work. We compare in Fig. 4 the pair interactions obtained from these two approaches. KRA model capture well the global features of these interactions, while, quantitatively, it overestimates such interactions (except T1-configuration for Al-C pair), leading to higher migration barriers of carbon atoms. Therefore, carbon diffusivity deduced from KRA model is smaller than that from *ab initio* database. As in Liu's work, their interactions of Si with carbon at tetrahedral sites are higher than those in our work, leading also to higher carbon migration barriers. This difference is due to the size effect mentioned in the first point.

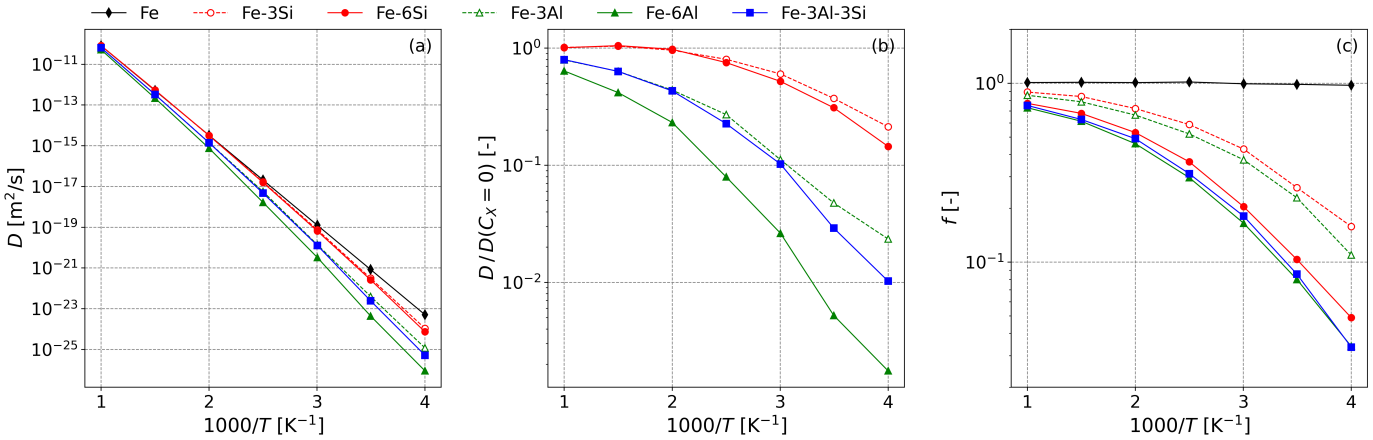

Figure 3: (a) Arrhenius plots of tracer carbon diffusion coefficients in bcc Fe, Fe-Si, Fe-Al and Fe-Al-Si systems. The alloy compositions are expressed in at.%. (b) Ratio between tracer diffusion coefficients of carbon in ferritic alloys and that of α-Fe. (c) Correlation factor of carbon in bcc Fe, Fe-Si, Fe-Al and Fe-Al-Si systems as a function of inverse temperature.

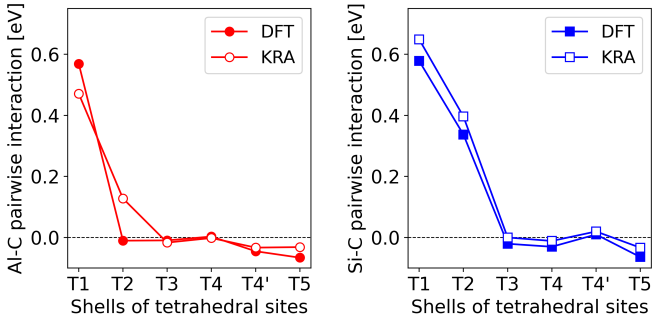

Figure 4: Pairwise interactions of carbon on tetrahedral positions with substitutional Al (left) and Si (right) obtained from DFT and KRA model.

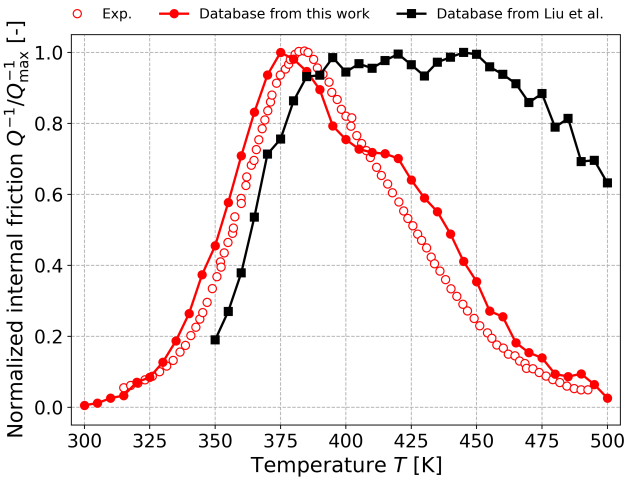

Figure 5: Experimental and simulated carbon Snoek relaxation profiles in bcc Fe-3Si (at.%). The experimental profile is reproduced from the work of Sinning et al. [17], in which the sample was water-quenched from 1000 K. The two simulated profiles were respectively obtained from the pair-interaction database of this work and the one of Liu et al. [8]. The experimental excitation frequency is 320–410 Hz, and the simulated one is set to 400 Hz.

Note that the signal of the internal friction is sensitive to the distribution of the migration enthalpy, which depends on the pairwise interaction database. In Fig. 5, we compare the simulated TDIF profiles in Fe-3Si using the database of this work and that of Liu et al. [8]. The experimental profile is also plotted as a reference result. As presented previously in Section 5.1, the simulated profile obtained from our *ab initio* energy database is in good agreement with the experimental profile. However, using Liu's database, we obtain a much wider TDIF profile. Moreover, the obtained peak position (around 420 K) does not correspond to the experimental peak (380 K). To this extent, our energy database has a higher reliability than that of Liu et al.

6.2. Short-range and long-range diffusion

The signal of internal friction results from one carbon jump. Thus, it characterizes the short-range diffusion behavior. However, in addition to the short-range atomic jumps, tracer diffusion also provides information on the long-range kinetic correlation. If the main difference between internal friction and tracer diffusion measurements is whether or not kinetic correlation is taken into account, the uncorrelated carbon diffusion coefficient (D_C/f_C) should be related to the relaxation peak of TDIF profile. Note that one can extract an effective migration enthalpy, H^m_{eff}, from the highest relaxation peak using Eq. (9). In Section 5.1, it is shown that H^m_{eff} is close to the most frequent jumps in the enthalpy distribution. From the Arrhenius fit of D_C/f_C, we can also obtain an effective migration enthalpy. We compare in Table 2 the effective migration enthalpies obtained from (a) the relaxation peak of internal friction profile, (b) the Arrhenius fit of the uncorrelated tracer diffusion coefficients, and (c) the Arrhenius fit of the correlated tracer diffusion coeffi-

cients in the investigated alloys. As expected, $H^{\mathrm{m}}_{\mathrm{eff}}$ from correlated diffusion is higher than those from the other two approaches because the solute-induced kinetic correlation decreases the carbon diffusivity. The $H^{\mathrm{m}}_{\mathrm{eff}}$ from internal friction profile corresponds relatively well with the one from uncorrelated diffusion, especially in Fe-3Si where the TDIF profile is nearly single-peaked. This quantitatively good agreement shows that one can roughly estimate the migration enthalpy of uncorrelated tracer diffusion from the internal friction measurement (with an error smaller than 0.03 eV in the investigated alloys). However, for a more complete study on the long-range diffusion behaviors, the tracer diffusion measurement is indispensable.

Table 2: Comparison of effective migration enthalpies (in eV) obtained from (a) the major relaxation peak of internal friction profile, (b) the Arrhenius fit of the uncorrelated tracer diffusion coefficients, and (c) the Arrhenius fit of the correlated tracer diffusion coefficients in Fe-3Si, Fe-6Al and Fe-3Si-3Al alloys.

Alloys	$H^{\mathrm{m}}_{\mathrm{eff}}$ (a)	$H^{\mathrm{m}}_{\mathrm{eff}}$ (b)	$H^{\mathrm{m}}_{\mathrm{eff}}$ (c)
Fe-3Si	0.87	0.87	0.92
Fe-6Al	0.99	0.96	1.05
Fe-3Si-3Al	0.93	0.91	1.00

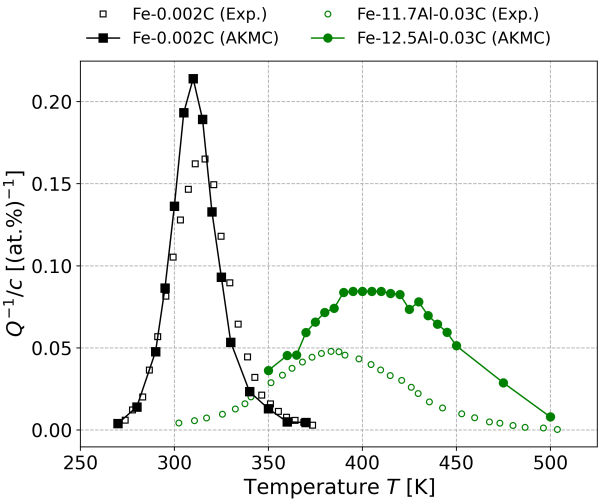

Figure 6: Experimental and simulated carbon Snoek relaxation profiles in α-Fe and bcc Fe-Al systems. The alloy compositions are expressed in at.% in the legend. The profiles are normalized by the carbon concentration (c). The excitation frequency is about 1 Hz in experiment and simulation. The experimental profile in α-Fe is reproduced from the results of Weller [42], and the one in Fe-11.7Al is from Golovin et al. [47].

6.3. Solute effect on the elastic parameters

Table 3: Elastic parameters of Fe-12.5Al (at.%) computed from first principles based on a SQS approach.

Lattice parameter [Å]	2.860
S_{11} [GPa^{-1}]	0.00836
S_{12} [GPa^{-1}]	−0.00307
S_{44} [GPa^{-1}]	0.00084
P^{O}, transverse [eV]	6.5
P^{O}, longitudinal [eV]	14.6
P^{T}, transverse [eV]	11.9
P^{T}, longitudinal [eV]	3.4

The introduction of concentrated substitutional solute atoms in ferrite can lead to significant modification of the elastic properties of the material. However, this point was not considered in the above presented simulation results because we mainly focus on the effect of short-range substitutional solute-carbon pair interactions on the carbon diffusion. The modification of the elastic parameters should not have remarkable effect on the carbon diffusion in ferrite because the carbon-induced strain is so small that it has negligible impacts on the carbon diffusion. However, a correct calculation of the elastic parameters is essential for the simulation of carbon kinetics in martensite (or body-centered tetragonal iron) [27, 48]. Note that the elastic parameters in concentrated alloys can be computed from first principles by building a Special Quasi-random Structure (SQS) [49]. We follow the same numerical scheme as presented in Ref. [20] to compute the elastic parameters of the bcc Fe-12.5Al (at.%) alloy (cf. Tab. 3), using the *mcsqs* module [50] of ATAT code [51]. Since the peak height of the internal friction profile is sensitive to the elastic parameters, the comparison between TDIF profiles from experimental measurement and those obtained from AKMC using the parameters in Tab. 3 provides a way to validate these parameters. The experimental and simulated profiles of α-Fe and Fe-Al systems are plotted in Fig. 6. To avoid the effect of the carbon concentration on the peak height, the TDIF profiles are normalized by the carbon content. We convert the simulated profile for a single crystal to the one for poly-crystal via the Reuss averaging method [52, 18]. According to the AKMC simulation the introduction of Al in α-Fe lowers the relaxation peak: the peak height in Fe-12.5Al is about one third of that in α-Fe. This decrease is consistent with what we observe from the experimental profiles. However, in both α-Fe and Fe-Al, the peaks of the simulated profiles are higher than those of the experimental profiles. This error may, on one hand, origin from the computed elastic parameters. On the other hand, the carbon content in the solid solution of the experimental specimens can be lower than the nominal value because, for instance, carbon atoms can be trapped in the Cottrell atmosphere around the dislocation. This unexpected decrease of the carbon content contributing to the internal friction in the experiment also leads to the discrepancy with the simulation results.

7. Conclusion

This work provides a multi-scale simulation of the short-range and long-range diffusion of carbon atoms in ferritic Fe-Si-C, Fe-Al-C and Fe-Al-Si-C alloys. First-principles calculations provide a database of the pairwise interaction of carbon atoms with neighboring substitutional solute atoms. Atomic kinetic Monte Carlo simulations are performed to calculate the internal friction profile and the tracer diffusion coefficients of carbon atoms. The most relevant results are summarized below.

- We obtain a good agreement between the simulated internal friction profile and the experimental one for an alloying solute up to 9 at.%. This consistency validates the pairwise interaction model which has been widely used to describe the local environment-dependent carbon migration.
- The comparison between the simulated and experimental internal friction profiles also provides a way to verify the database of the pairwise interaction energy.
- Al is much more efficient than Si in slowing down carbon diffusion because Al has more attractive neighboring shells, which leads to a more remarkable kinetic trapping of carbon atoms.
- We highlight a super-cell size effect on the short-range Si-C pair interactions resulting from first-principles calculations. Increasing the size of super-cell changes the sign of certain pair interactions. According to our energy database, the introduction of 3 at% and 9 at% Si in ferrite slightly increases the carbon diffusivity at above 500 K, which is unexpected by previous studies.

Acknowledgments

This work was supported by the Agence Nationale de la Recherche (contract C-TRAM ANR-18-CE92–0021). Centre de Calcul Intensif d'Aix-Marseille is acknowledged for granting access to its high performance computing resources. The authors thank Prof. I. S. Golovin for fruitful discussions and valuable comments.

Data availability

The authors confirms that the data supporting the findings of this study are available within the article. Raw data that support the findings of this study are available from the corresponding author, upon reasonable request.

References

[1] D. Ruiz, J. L. Rivera-Tovar, D. Segers, R. E. Vandenberghe, Y. Houbaert, Aging phenomena in high-Si steels studied by internal friction, Mater. Sci. Eng. A 442 (1-2 SPEC. ISS.) (2006) 462–465. doi:10.1016/j.msea.2006.05.164.

[2] C. S. Becquart, J. M. Raulot, G. Bencteux, C. Domain, M. Perez, S. Garruchet, H. Nguyen, Atomistic modeling of an Fe system with a small concentration of C, Comput. Mater. Sci. 40 (1) (2007) 119–129. doi:10.1016/j.commatsci.2006.11.005.

[3] K. TAPASA, A. BARASHEV, D. BACON, Y. OSETSKY, Computer simulation of carbon diffusion and vacancy–carbon interaction in α-iron, Acta Mater. 55 (1) (2007) 1–11. doi:10.1016/j.actamat.2006.05.029.
URL https://linkinghub.elsevier.com/retrieve/pii/S1359645406003703

[4] I. S. Golovin, S. B. Golovina, O. A. Sokolova, Effect of thermal aging on the temperature spectrum of internal friction of alloyed Fe-Si-Al-C ferrite, Phys. Met. Metallogr. 105 (2) (2008) 193–201. doi:10.1007/s11508-008-2012-6.

[5] F. Walz, T. Wakisaka, H. Kronmüller, Kinetics of carbon precipitation and re-solution in low Si-content silicon iron, Phys. Status Solidi Appl. Mater. Sci. 202 (14) (2005) 2667–2678. doi:10.1002/pssa.200520081.

[6] A. Strahl, I. Golovin, H. Neuhäuser, S. Golovina, H.-R. Sinning, Influence of Al concentration on the short-range and long-range diffusion of carbon in Fe–Al alloys, Mater. Sci. Eng. A 442 (1-2) (2006) 128–132. doi:10.1016/j.msea.2006.05.160.
URL https://linkinghub.elsevier.com/retrieve/pii/S0921509306010446

[7] D. Simonovic, C. K. Ande, A. I. Duff, F. Syahputra, M. H. F. Sluiter, Diffusion of carbon in bcc Fe in the presence of Si, Phys. Rev. B 81 (5) (2010) 054116. doi:10.1103/PhysRevB.81.054116.
URL https://link.aps.org/doi/10.1103/PhysRevB.81.054116

[8] P. Liu, W. Xing, X. Cheng, D. Li, Y. Li, X. Q. Chen, Effects of dilute substitutional solutes on interstitial carbon in α -Fe: Interactions and associated carbon diffusion from first-principles calculations, Phys. Rev. B - Condens. Matter Mater. Phys. 90 (2) (2014) 1–14. doi:10.1103/PhysRevB.90.024103.

[9] D. Hasson, R. Arsenault, Substitutional-Interstitial Interactions in bcc Alloys, in: Treatise Mater. Sci. Technol., Princeton University Press, 1972, pp. 179–246. doi:10.1016/B978-0-12-341801-2.50009-6.
URL https://www.degruyter.com/document/doi/10.1515/9781400832460-013/htmlhttps://linkinghub.elsevier.com/retrieve/pii/B9780123418012500096

[10] I. S. Golovin, M. S. Blanter, T. V. Pozdova, K. Tanaka, L. B. Magalas, Effect of substitutional ordering on the carbon snoek relaxation in Fe-Al-C alloys, Phys. Status Solidi Appl. Res. 168 (2) (1998) 403–415. doi:10.1002/(SICI)1521-396X(199808)168:2<403::AID-PSSA403>3.0.CO;2-2.

[11] T. Pozdova, I. Golovin, Mechanical spectroscopy of Fe-Al-C alloys ordering, Solid State Phenom. 89 (2003) 279–286. doi:10.4028/www.scientific.net/ssp.89.279.

[12] I. S. Golovin, H. Neuhäuser, A. Rivière, A. Strahl, Anelasticity of Fe-Al alloys, revisited, Intermetallics 12 (2) (2004) 125–150. doi:10.1016/j.intermet.2003.10.003.

[13] H. Saitoh, N. Yoshinaga, K. Ushioda, Influence of substitutional atoms on the Snoek peak of carbon in b.c.c. iron, Acta Mater. 52 (5) (2004) 1255–1261. doi:10.1016/j.actamat.2003.11.009.

[14] I. S. Golovin, S. B. Golovina, Effect of alloying α-Fe with aluminum, silicon, cobalt, and germanium on the snoek relaxation parameters, Phys. Met. Metallogr. 102 (6) (2006) 593–603. doi:10.1134/S0031918X06120064.

[15] M. S. Blanter, I. S. Golovin, H. Neuhäuser, H.-R. Sinning, Internal Friction in Metallic Materials, Vol. 90 of Springer Series in Materials Science, Springer Berlin Heidelberg, Berlin, Heidelberg, 2007. doi:10.1007/978-3-540-68758-0.
URL http://link.springer.com/10.1007/978-3-540-68758-0

[16] I. S. Golovin, S. Jäger, V. A. Semin, G. V. Serzhantova, H. R. Sinning, O. A. Sokolova, F. Stein, S. A. Golovin, Snoek-type and Zener relaxation in Fe-Si-Al Alloys, Solid State Phenom. 137

(2008) 69–82. doi:10.4028/www.scientific.net/SSP.137.69.
[17] H. R. Sinning, I. S. Golovin, A. Strahl, O. A. Sokolova, T. Sazonova, Interactions between solute atoms in Fe-Si-Al-C alloys as studied by mechanical spectroscopy, Mater. Sci. Eng. A 521-522 (2009) 63–66. doi:10.1016/j.msea.2008.09.110.
[18] A. S. Nowick, B. Berry, Anelastic Relaxation in Crystalline Solids, Elsevier, 1972. doi:10.1016/B978-0-12-522650-9.X5001-0.
URL https://linkinghub.elsevier.com/retrieve/pii/B9780125226509X50010
[19] R. Herschberg, C.-C. Fu, M. Nastar, F. Soisson, Atomistic modelling of the diffusion of C in Fe Cr alloys, Acta Materialia 165 (2019) 638–653. doi:10.1016/j.actamat.2018.11.025.
URL https://doi.org/10.1016/j.actamat.2018.11.025https://linkinghub.elsevier.com/retrieve/pii/S1359645418309017
[20] P. Eyméoud, L. Huang, P. Maugis, Impact of Ni alloying on Fe-C martensite ageing: an atomistic investigation, Scr. Mater. 205 (2021) 114182. doi:10.1016/j.scriptamat.2021.114182.
URL https://linkinghub.elsevier.com/retrieve/pii/S1359646221004620
[21] T. Schuler, L. Messina, M. Nastar, KineCluE: A kinetic cluster expansion code to compute transport coefficients beyond the dilute limit, Comput. Mater. Sci. 172 (May 2019) (2020) 109191. doi:10.1016/j.commatsci.2019.109191.
URL https://doi.org/10.1016/j.commatsci.2019.109191https://linkinghub.elsevier.com/retrieve/pii/S0927025619304902
[22] O. Buggenhoudt, T. Schuler, C.-C. Fu, J.-L. Béchade, Predicting carbon diffusion in cementite from first principles, Phys. Rev. Mater. 5 (6) (2021) 063401. doi:10.1103/PhysRevMaterials.5.063401.
URL https://link.aps.org/doi/10.1103/PhysRevMaterials.5.063401
[23] S. Garruchet, M. Perez, Modelling the carbon snoek peak in ferrite: coupling molecular dynamics and kinetic monte-carlo simulations, Comput. Mater. Sci. 43 (2) (2008) 286–292. doi:10.1016/j.commatsci.2007.11.004.
URL https://linkinghub.elsevier.com/retrieve/pii/S0927025607003254
[24] V. Dmitriev, M. Blanter, A. Ruban, B. Johansson, Ab initio based investigation of interstitial interactions and Snoek relaxation in Nb–O, J. Phys. Chem. Solids 73 (2) (2012) 182–187. doi:10.1016/j.jpcs.2011.11.008.
URL http://dx.doi.org/10.1016/j.jpcs.2011.11.008https://linkinghub.elsevier.com/retrieve/pii/S0022369711003866
[25] L. Huang, P. Maugis, Effect of substitutional Ni atoms on the Snoek relaxation in ferrite and martensite Fe-C alloys: An atomisitic investigation, Comput. Mater. Sci. 203 (December 2021) (2022) 111083. doi:10.1016/j.commatsci.2021.111083.
URL https://doi.org/10.1016/j.commatsci.2021.111083https://linkinghub.elsevier.com/retrieve/pii/S0927025621007539
[26] A. Khachaturyan, G. Shatalov, On the theory of the ordering of carbon atoms in a martensite crytal, Physics of Metals and Metallography 32 (1971) 1–9.
[27] P. Maugis, Ferrite, martensite and supercritical iron: A coherent elastochemical theory of stress-induced carbon ordering in steel, Acta Materialia 158 (2018) 454–465. doi:10.1016/j.actamat.2018.08.001.
URL https://doi.org/10.1016/j.actamat.2018.08.001https://linkinghub.elsevier.com/retrieve/pii/S1359645418306256
[28] C. Varvenne, F. Bruneval, M.-C. Marinica, E. Clouet, Point defect modeling in materials: Coupling ab initio and elasticity approaches, Physical Review B 88 (13) (2013) 134102. doi:10.1103/PhysRevB.88.134102.
URL https://link.aps.org/doi/10.1103/PhysRevB.88.134102
[29] B. Lawrence, C. W. Sinclair, M. Perez, Carbon diffusion in supersaturated ferrite: a comparison of mean-field and atomistic predictions, Model. Simul. Mater. Sci. Eng. 22 (6) (2014) 065003. doi:10.1088/0965-0393/22/6/065003.
URL https://iopscience.iop.org/article/10.1088/0965-0393/22/6/065003
[30] E. Clouet, C. Varvenne, T. Jourdan, Elastic modeling of point-defects and their interaction, Comput. Mater. Sci. 147 (2018) 49–63. arXiv:1802.04062, doi:10.1016/j.commatsci.2018.01.053.
URL https://doi.org/10.1016/j.commatsci.2018.01.053
[31] G. Kresse, J. Furthmüller, Efficiency of ab-initio total energy calculations for metals and semiconductors using a plane-wave basis set, Comput. Mater. Sci. 6 (1) (1996) 15–50. doi:10.1016/0927-0256(96)00008-0.
URL https://linkinghub.elsevier.com/retrieve/pii/0927025696000080
[32] G. Kresse, J. Furthmüller, Efficient iterative schemes for ab initio total-energy calculations using a plane-wave basis set, Phys. Rev. B 54 (16) (1996) 11169–11186. doi:10.1103/PhysRevB.54.11169.
URL https://link.aps.org/doi/10.1103/PhysRevB.54.11169
[33] G. Krauss, Martensite in steel: strength and structure, Mater. Sci. Eng. A 273-275 (1999) 40–57. doi:10.1016/S0921-5093(99)00288-9.
URL https://linkinghub.elsevier.com/retrieve/pii/S0921509399002889
[34] P. E. Blöchl, Projector augmented-wave method, Phys. Rev. B 50 (24) (1994) 17953–17979. doi:10.1103/PhysRevB.50.17953.
URL https://link.aps.org/doi/10.1103/PhysRevB.50.17953
[35] J. P. Perdew, K. Burke, M. Ernzerhof, Generalized Gradient Approximation Made Simple, Phys. Rev. Lett. 77 (18) (1996) 3865–3868. doi:10.1103/PhysRevLett.77.3865.
URL https://link.aps.org/doi/10.1103/PhysRevLett.77.3865
[36] J. P. Perdew, K. Burke, M. Ernzerhof, Generalized Gradient Approximation Made Simple [Phys. Rev. Lett. 77, 3865 (1996)], Phys. Rev. Lett. 78 (7) (1997) 1396–1396. doi:10.1103/PhysRevLett.78.1396.
URL https://link.aps.org/doi/10.1103/PhysRevLett.78.1396
[37] H. J. Monkhorst, J. D. Pack, Special points for Brillouin-zone integrations, Phys. Rev. B 13 (12) (1976) 5188–5192. doi:10.1103/PhysRevB.13.5188.
URL https://link.aps.org/doi/10.1103/PhysRevB.13.5188
[38] A. Bakaev, D. Terentyev, G. Bonny, T. Klaver, P. Olsson, D. Van Neck, Interaction of minor alloying elements of high-Cr ferritic steels with lattice defects: An ab initio study, J. Nucl. Mater. 444 (1-3) (2014) 237–246. doi:10.1016/j.jnucmat.2013.09.053.
URL http://dx.doi.org/10.1016/j.jnucmat.2013.09.053https://linkinghub.elsevier.com/retrieve/pii/S0022311513011306
[39] A. A. Mirzoev, Y. M. Ridnyi, A. V. Verkhovykh, Ab initio Computer Simulation of the Energy Parameters and the Magnetic Effects in Ternary Fe–X–C (X = Si, P, S, Cr, Mn) Systems, Russ. Metall. 2019 (2) (2019) 168–172. doi:10.1134/S0036029519020174.
URL http://link.springer.com/10.1134/S0036029519020174
[40] J. da Silva, R. B. McLellan, Diffusion of carbon and nitrogen in B.C.C. iron, Materials Science and Engineering 26 (1) (1976) 83–87. doi:10.1016/0025-5416(76)90229-9.
URL https://linkinghub.elsevier.com/retrieve/pii/0025541676902299
[41] P. Maugis, Thermo-kinetic modelling of the giant Snoek effect in carbon-supersaturated iron, Journal of Alloys and Compounds 877 (2021) 160236. doi:10.1016/j.jallcom.2021.160236.
URL https://linkinghub.elsevier.com/retrieve/pii/S0925838821016455
[42] M. Weller, The Snoek relaxation in bcc metals—From steel wire to meteorites, Materials Science and Engineering: A 442 (1-2) (2006) 21–30. doi:10.1016/j.msea.2006.02.232.

URL https://linkinghub.elsevier.com/retrieve/pii/S092150930601166X

[43] S. A. Golovin, I. S. Golovin, Mechanical spectroscopy of snoek type relaxation, Met. Sci. Heat Treat. 54 (5-6) (2012) 208–216. doi:10.1007/s11041-012-9483-6.

[44] O. Lambri, B. Weidenfeller, F. Bonifacich, J. Pérez-Landazábal, G. Cuello, L. Weidenfeller, V. Recarte, G. Zelada, W. Riehemann, Magnetic behavior in commercial iron-silicon alloys controlled by the dislocation dynamics at temperatures below 420 K, J. Alloys Compd. 856 (2021) 157934. doi:10.1016/j.jallcom.2020.157934.
URL https://linkinghub.elsevier.com/retrieve/pii/S0925838820342985

[45] J.-Y. Yan, A. Ruban, Configurational thermodynamics of C in body-centered cubic/tetragonal Fe: A combined computational study, Comput. Mater. Sci. 147 (2018) 293–303. doi:10.1016/j.commatsci.2018.02.024.
URL https://doi.org/10.1016/j.commatsci.2018.02.024https://linkinghub.elsevier.com/retrieve/pii/S0927025618301071

[46] A. Van der Ven, G. Ceder, M. Asta, P. D. Tepesch, First-principles theory of ionic diffusion with nondilute carriers, Phys. Rev. B 64 (18) (2001) 184307. doi:10.1103/PhysRevB.64.184307.
URL https://link.aps.org/doi/10.1103/PhysRevB.64.184307

[47] I. S. Golovin, T. V. Pozdova, N. Y. Rokhmanov, D. Mukherji, Relaxation mechanisms in Fe-Al-C alloys, Metall. Mater. Trans. A Phys. Metall. Mater. Sci. 34 (2) (2003) 255–266. doi:10.1007/s11661-003-0327-2.

[48] P. Maugis, S. Chentouf, D. Connétable, Stress-controlled carbon diffusion channeling in bct-iron: A mean-field theory, J. Alloys Compd. 769 (2018) 1121–1131. doi:10.1016/j.jallcom.2018.08.060.
URL https://linkinghub.elsevier.com/retrieve/pii/S0925838818329335

[49] A. Zunger, S.-H. Wei, L. G. Ferreira, J. E. Bernard, Special quasirandom structures, Phys. Rev. Lett. 65 (3) (1990) 353–356. doi:10.1103/PhysRevLett.65.353.
URL https://link.aps.org/doi/10.1103/PhysRevLett.65.353

[50] A. van de Walle, P. Tiwary, M. de Jong, D. Olmsted, M. Asta, A. Dick, D. Shin, Y. Wang, L.-Q. Chen, Z.-K. Liu, Efficient stochastic generation of special quasirandom structures, Calphad 42 (2013) 13–18. doi:10.1016/j.calphad.2013.06.006.
URL https://linkinghub.elsevier.com/retrieve/pii/S0364591613000540

[51] A. van de Walle, M. Asta, G. Ceder, The alloy theoretic automated toolkit: A user guide, Calphad 26 (4) (2002) 539–553. doi:10.1016/S0364-5916(02)80006-2.
URL https://linkinghub.elsevier.com/retrieve/pii/S0364591602800062

[52] H. Ino, S. Takagi, T. Sugeno, On the relaxation strength of the snoek peak, Acta Metallurgica 15 (1) (1967) 29–34. doi:10.1016/0001-6160(67)90152-6.
URL https://linkinghub.elsevier.com/retrieve/pii/0001616067901526